

In vivo delivery of gene therapy to tumours

L. R. Band, R. J. S. Booth, L. J. Cummings, R. J. Dyson,
K. D. Fisher, I. M. Griffiths, J. P. Moles & S. L. Waters

August 11, 2006

Abstract

In gene therapy, tumour growth is inhibited by viruses which are delivered to the tumour via the blood stream. This therapy utilises the leakiness of the tumour capillaries, which enables virus particles to pass through gaps between the endothelial cells. Our models assess the key influences on the number of virus particles which enter the tumour. We model on both the macroscale, where we represent the tumour as a porous medium, and on the cellular scale, where we consider a single virus particle entering a single gap. In both models, a proportion of the virus particles are found to enter the tumour. Several types of virus particle can be used for the therapy, and the size and physical characteristics of the virus particle will affect its interactions with the blood flow. In particular, the fluid stresses on an encapsulated virus particle cause the particle to deform. These deformations influence the virus particle's position within the capillary which in turn is likely to affect the number of virus particles that enter the tumour.

1 Introduction

Cancer-specific viruses are able to replicate inside tumour cells and destroy them [9]. In early clinical trials viruses have been injected straight into a single tumour nodule; these trials exhibit encouraging anti-cancer activity and regression of the tumour. However, the virus is unable to spread between the disseminated tumour masses, therefore this technique is limited to isolated tumours. Unfortunately, most common cancer types present with multiple metastatic tumours and it is often impractical to inject viruses into each tumour nodule. Virus particles are generally not compatible with intravenous administration because they are rapidly cleared by the immune system.

The group led by Dr Len Seymour in the Department of Clinical Pharmacology at Oxford, has devised a novel way of treating virus particles with polymers to ensure the particles are less susceptible to attack by the host immune system [3]. These polymer-coated vectors are able to circulate in the blood stream for sufficient time to reach distant tumours [5].

Functional capillaries exist in the proliferating zone toward the edge of the tumour. The leaky vasculature associated with tumour structure lends itself to accumulation of virus particles delivered via the blood stream. Unlike the continuous endothelium of most normal tissues, the endothelial cells of tumour capillaries are discontinuous, with large

gaps between cells [2]. The mean pressure in such a capillary is 15 – 35 mmHg (1 mmHg = $133.322 \text{ kg m}^{-1}\text{s}^{-2}$), the mean pressure in the tumour is about 15 mmHg and the mean pressure in the draining blood capillaries is about 2 mmHg. Thus, due to the driving pressure gradient, fluid and virus particles leave the capillary through the gaps between the endothelial cells and enter the tumour stroma (the fluid bathing the tumour cells). Small molecules such as water percolate through the tumour structure and leave through the draining blood capillaries, but large particles are trapped in the tumour stroma by a network of extracellular matrix proteins, effectively filtering and concentrating virus particles [8].

Gene therapy may be delivered from a range of blood vessels; the leakiest vessels (and therefore potentially the most useful for the present application) are the capillaries supplying the tumour (radii 2.5 – 50 μm), although arterioles (radii 0.05 – 1 mm) which pass through tumour tissues may also be leaky in places. In general therefore a range of blood flow rates must be considered, though here we focus on the flow within a single capillary, and so use parameter values appropriate to this situation. In a capillary the endothelial gaps vary from around 50 to 1000 nm in diameter, and occur with variable spatial frequency.

Many parameters may influence the number of virus particles entering the tumour, not least the type of virus used. Examples of viruses used by the Seymour group include the *adenovirus* and the *vaccinia poxvirus*. The adenovirus is small and rigid, with radius $r_v \approx 100 \text{ nm}$. It can be coated with a hydrophilic polymer which, depending upon the amount of coating, can make the surface of the virus either rigid or highly deformable. Alternatively, the vaccinia poxvirus is larger, with radius $r_v \approx 350 \text{ nm}$. It has a small hard centre (the core) surrounded by a fluid region (the tegument), which in turn is surrounded by a loose membrane. The vaccinia poxvirus may also be coated, but the influence of the coating on the deformability of the particle remains to be studied. We focus on these two virus particles, as typifying two extreme types in both size and physical characteristics. They will henceforth be referred to as the *small rigid* and the *large encapsulated* virus particles respectively. Such different virus types will obviously behave differently in the blood flow, and hence the likelihood of virus particles entering an endothelial gap will depend on the virus used.

This report aims to provide insight into the possible efficacy of the virus delivery method. We consider virus particles flowing through the tumour in a single capillary. When modelling blood flow on this scale a major issue is the influence of the red blood cells. Red blood cells occupy approximately 50% of the blood volume and have diameters of approximately 8 μm , thus are considerably larger than the virus particles (and could fill up the entire vessel lumen). The red blood cells will certainly affect the transport of the viruses through the endothelium and into the tumour, though for simplicity, throughout this report the red blood cells are neglected and the fluid inside the capillaries is taken to be blood plasma. We note however that further study is clearly needed to take account of the effect of blood composition.

The report structure is as follows. In §2 we estimate the size of various relevant dimensionless parameters in the problem. In §3 we consider the macroscale problem of flow through an entire tumour. We model the tumour as a porous medium with a capillary passing through it. We assume the virus particles are advected with the blood flow and assess the amount of blood (and virus particles) which leaks from the capillary into the

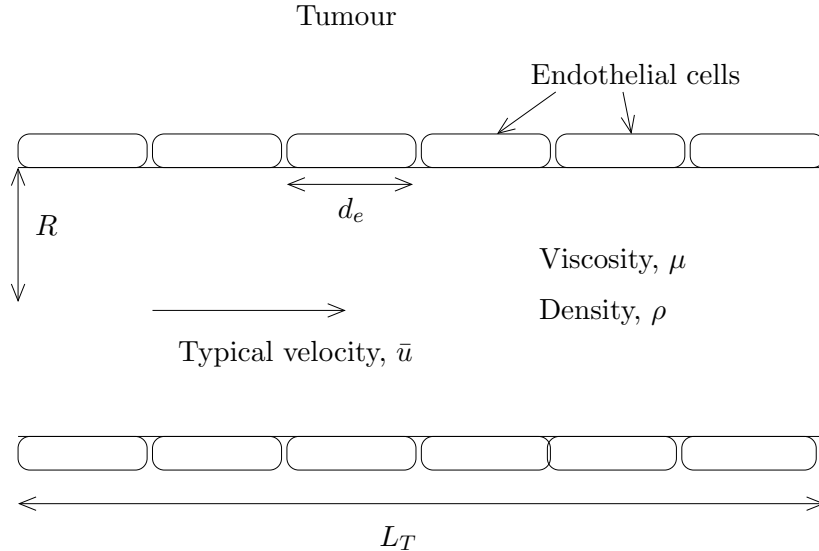


FIGURE 1: Diagram to show the parameters.

tumour. We focus on a smaller length scale in §4, considering the local flow into a single gap between endothelial cells. In §4.1 the virus particles are taken to be point particles, which are simply advected with the flow. In this case it is sufficient to solve for the flow in a tube with a single side-branch at lower pressure. This problem was considered by Tutty [10], and his solutions can therefore be used to determine the virus particle capture in this situation. However there is a range of possible gap sizes; in §4.2 we assume the size of a small rigid virus particle is comparable to the size of the gap, and therefore its interaction with the flow is important. In this more complicated problem, we consider only a single (rigid spherical) particle within the flow. The relevant fluid dynamical problem was addressed by Wu *et al.* [11]. In both these cases the initial position of the virus particle(s) within the capillary determines whether it enters the endothelial gap (and thus the tumour). However an encapsulated virus will behave very differently to a rigid virus. In §5 we briefly consider how the physical properties of a large encapsulated virus affect the motion of the virus particle when it is close to the vessel wall.

2 Estimation of dimensionless parameters

We model blood plasma as a Newtonian fluid with kinematic viscosity $\mu = 1.35 \times 10^{-3} \text{ kg m}^{-1} \text{ s}^{-2}$ and density $\rho = 1060 \text{ kg m}^{-3}$. In the axial direction along a typical capillary, the mean velocity of blood is between $0.1 \times 10^{-3} \text{ ms}^{-1}$ and $15 \times 10^{-3} \text{ ms}^{-1}$, thus we take a typical axial capillary velocity to be $\bar{u} = 1 \times 10^{-3} \text{ ms}^{-1}$. There are several length scales of interest, illustrated in figure 1. We take a typical tumour (and capillary) length to be $L = 0.025 \text{ m}$ and the typical distance between endothelial gaps to be the maximum diameter of an endothelial cell, $d_e = 20 \mu\text{m}$. All our models are relevant to a capillary with radius $R \approx 2.5 \mu\text{m}$. The aspect ratio of the capillary is then $\epsilon = R/L \sim 1 \times 10^{-4}$. The virus radius r_v will be taken to be 100 nm for the small virus, and 350 nm for the large virus.

The Reynolds number for the flow based upon the tumour/capillary lengthscale is

$$\text{Re}_{\text{cap}} = \frac{\bar{u}L\rho}{\mu} \approx 20. \quad (2.1)$$

The reduced Reynolds number is then $\epsilon^2\text{Re}_{\text{cap}} = 2.0 \times 10^{-7}$, thus lubrication theory is applicable to flow in the capillary (note that this assumes that the endothelial gaps do not greatly disturb the axial flow in the capillary, so that L is indeed an appropriate lengthscale for the axial flow).

For flow into a single gap in the endothelium the Reynolds number is

$$\text{Re}_{\text{gap}} = \frac{\bar{u}d_e\rho}{\mu} = 0.016 \ll 1, \quad (2.2)$$

therefore for the local problems considered in §4 inertia can be neglected.

In §4.2, the presence of a small rigid virus particle influences the blood flow close to the gap, therefore we also have a particle Reynolds number given by

$$\text{Re}_{\text{part}} = \frac{\bar{u}r_v\rho}{\mu} = 7.9 \times 10^{-5} \quad \text{for the small virus particles.} \quad (2.3)$$

The diffusion coefficient of the virus particles is given by

$$D = \frac{k_B T}{6\pi\mu r_v}, \quad (2.4)$$

where $k_B = 1.38 \times 10^{-23} \text{ JK}^{-1}$ is the Boltzmann constant, and $T = 310 \text{ K}$ is the temperature of the blood. On the length scale of the tumour/capillary the Peclet numbers (which measure the relative importance of advection and diffusion) for each of the virus particles are

$$P_e = \frac{\bar{u}L}{D} = 1.5 \times 10^7 \quad \text{for the small virus particles.} \quad (2.5)$$

however the reduced Peclet numbers based on the capillary radius, $\epsilon^2 P_e$, are 0.15 and 0.52 for the small and the large virus particles respectively. To enter an endothelial gap particles have only to traverse the width of the capillary, thus for the large virus particle we must consider the combined effects of advection and diffusion.

3 Flow through a capillary

3.1 Introduction

In this section we derive a model for flow through a capillary within a tumour. For simplicity, since we seek only order-of-magnitude estimates for the degree of virus capture, we consider a two-dimensional Cartesian coordinate system (x, y) in which the capillary is represented as a straight channel, $0 \leq x \leq L$, $-R \leq y \leq R$, surrounded by tumour tissue occupying $R \leq |y| \leq R_T$. We assume symmetry about the channel centreline $y = 0$, thus we need only consider flow in $0 \leq x \leq L$, $0 \leq y \leq R_T$. See figure 2 for a schematic.

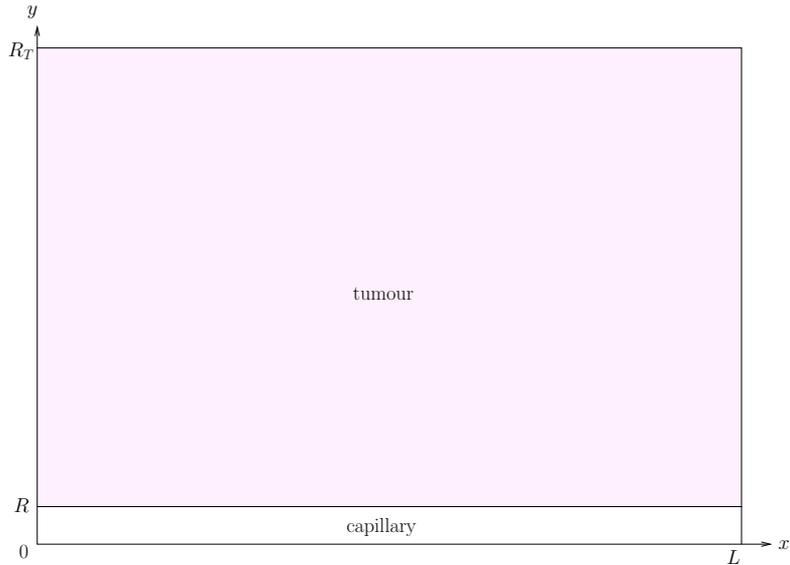


FIGURE 2: Schematic diagram for the model of the entire tumour.

We assume the thickness of the endothelium is sufficiently small (relative to R) that we may consider both capillary and tumour interfaces to be at $y = R$. The blood is at pressure $p(x, y, t)$ and has viscosity μ ; it flows into the capillary at $x = 0$, with a velocity $\mathbf{u} = \mathbf{u}(x, y, t) = u(x, y, t)\hat{\mathbf{x}} + v(x, y, t)\hat{\mathbf{y}}$, driven by the pressure drop along the capillary. We model the tumour as a porous medium with permeability k , pressure $p_T(x, y, t)$ and fluid velocity $\mathbf{u}_T(x, y, t) = u_T(x, y, t)\hat{\mathbf{x}} + v_T(x, y, t)\hat{\mathbf{y}}$. The fluid surrounding the tumour is at the pressure of the draining blood capillaries and, without loss of generality, we set this equal to zero. We consider two different boundary conditions for this model, and compare these two approaches by assessing their applicability to the biological problem and their mathematical limitations.

For simplicity, we neglect the diffusion of the virus particles and assume they are merely advected by the blood flow (but note that the relevant Peclet number may be $O(1)$ as shown in §2 above, therefore including diffusion would be a valuable extension to this model). We are particularly interested in the quantity of fluid that will leak out of the capillary into the tumour, as this enables us to estimate the proportion of injected virus particles that will enter the tumour. Two possible simple models for this problem are considered in turn, and their relative merits briefly discussed.

3.2 Model 1

The flow in the capillary is governed by the continuity and Navier Stokes equations. Incompressible flow in the tumour is governed by Darcy's law

$$\nabla \cdot \mathbf{u}_T = 0, \quad \mathbf{u}_T = -\frac{k}{\mu} \nabla p_T, \quad (3.1a,b)$$

which gives

$$\nabla^2 p_T = 0. \quad (3.2)$$

We would typically specify the upstream flux into the capillary, Q . However, at the capillary entrance, the flux is directly proportional to the pressure gradient (see (3.23)), and, for convenience, we prescribe here the pressure gradient,

$$\frac{\partial p(0, y)}{\partial x} = -G, \quad \text{for } 0 \leq y \leq R, \quad (3.3)$$

where G is a constant.

As well as the driving condition (3.3) at the capillary entrance, we impose symmetry conditions on the channel centreline

$$\frac{\partial u}{\partial y} = 0, \quad v = 0, \quad \text{for } y = 0, 0 \leq x \leq L. \quad (3.4a,b)$$

At the interface between the capillary and the tumour we assume continuity of pressure and normal velocity, and we also impose a third slip condition on the tangential velocity (first proposed by Beavers & Joseph [1]), thus

$$v = v_T, \quad p = p_T, \quad \frac{\partial u}{\partial y} = -\frac{\alpha}{\sqrt{k}}(u - u_T), \quad \text{on } y = R. \quad (3.5a-c)$$

The dimensionless quantity α in (3.5c) characterises the structure of the permeable material within the boundary region [1], and k represents the permeability of the endothelial cells that form the capillary wall; however we assume that this is the same as the permeability of the tumour.

On the external tumour boundaries we should apply continuity of pressure, thus

$$p_T(x, R_T) = 0, \quad \text{for } 0 \leq x \leq L, \quad (3.6)$$

and

$$p_T(L, y) = 0, \quad \text{for } 0 \leq y \leq R_T. \quad (3.7)$$

However, if we also apply $p_T(0, y) = 0$ for $R \leq y \leq R_T$ there is a discontinuity in pressure at $(0, R)$; therefore on the boundary at $x = 0$ we expect a boundary layer, lying between (say) $0 \leq x \leq x^*$, $R \leq y \leq R_T$, for some $0 < x^* \ll L$. Consequently, we will not impose a boundary condition on the interface between the boundary layer and the main tumour domain, but let this be part of the solution for p_T in $x^* \leq x \leq L$, $R \leq y \leq R_T$. Due to continuity of pressure across the capillary-tumour interface, by prescribing boundary conditions (3.3) and (3.7) there is a pressure gradient along the capillary which drives flow.

3.2.1 Asymptotic analysis

We nondimensionalise the system, exploiting the small aspect ratio $\epsilon = R/L$ and employing lubrication scalings in the capillary. Continuity of pressure and normal velocity at the tumour-capillary interface determines the scalings for the pressure, p_T , and the normal velocity v_T of the fluid in the tumour. By continuity, the normal and tangential velocity components of the flow in the tumour are the same order. We thus scale as follows,

$$\begin{aligned} x &= Lx', & y &= Ly' = \epsilon LY, & u &= \bar{u}u', & v &= \epsilon \bar{u}v', \\ u_T &= \epsilon \bar{u}u'_T, & v_T &= \epsilon \bar{u}v'_T, & p &= \frac{\mu \bar{u}}{\epsilon^2 L} p', & p_T &= \frac{\mu \bar{u}}{\epsilon^2 L} p'_T, \end{aligned} \quad (3.8)$$

where \bar{u} denotes the mean axial fluid velocity in the capillary at $x = 0$. The leading-order governing equations for the capillary become, dropping dashes for convenience,

$$\frac{\partial u}{\partial x} + \frac{\partial v}{\partial Y} = 0, \quad \frac{\partial p}{\partial Y} = 0, \quad \frac{\partial^2 u}{\partial Y^2} = \frac{\partial p}{\partial x}, \quad (3.9a-c)$$

and those for the tumour fluid become

$$\frac{\partial u_T}{\partial x} + \frac{\partial v_T}{\partial y} = 0, \quad (3.10)$$

$$u_T = -\mathcal{K} \frac{\partial p_T}{\partial x}, \quad v_T = -\mathcal{K} \frac{\partial p_T}{\partial y}, \quad (3.11a,b)$$

$$\frac{\partial^2 p_T}{\partial x^2} + \frac{\partial^2 p_T}{\partial y^2} = 0, \quad (3.12)$$

where $\mathcal{K} = kL/R^3$ is a dimensionless tumour permeability.

The leading-order boundary conditions are:

$$\frac{\partial u}{\partial Y} = 0, \quad v = 0, \quad \text{on } Y = 0; \quad (3.13a,b)$$

$$v = v_T, \quad p = p_T, \quad \frac{\partial u}{\partial Y} = -\mathcal{A}u, \quad \text{on } y = 0, Y = 1, \quad (3.14a-c)$$

where $\mathcal{A} = \alpha R/\sqrt{k}$;

$$p_T(1, y) = 0, \quad \text{for } 0 \leq y \leq \mathcal{R}_T,$$

where $\mathcal{R}_T = R_T/L$;

$$p_T(x, \mathcal{R}_T) = 0, \quad \text{for } 0 \leq x \leq 1; \quad (3.15)$$

and

$$\frac{\partial p(0, Y)}{\partial x} = -\mathcal{G}, \quad \text{for } 0 \leq Y \leq 1, \quad (3.16)$$

where $\mathcal{G} = R^2 G/\mu \bar{u}$.

3.2.2 Typical parameter values

Experimental observations could be found only for the ‘vascular permeability’, that is the permeability of the whole tumour including the arteries and capillaries within. We estimate the permeability of the tumour tissue by modelling the space between tumour cells as a tubular network. If the fraction of pore space is given by ϕ , and the mean cell size is given by d , then (see [4]) the permeability

$$k \approx \frac{\phi^2 d^2}{72\pi}. \quad (3.17)$$

The size and spacing of tumour cells is comparable with the size and spacing of endothelial cells. With $d = 5 \mu\text{m}$ and an intercellular spacing of $0.5 \mu\text{m}$, we find that $\phi \approx 0.25$, giving a permeability $k \sim 10^{-14} \text{m}^2$.

Using values $R = 2.5 \mu\text{m}$ (a typical capillary radius), $L = 2.5 \text{ cm}$ (a typical tumour width), $k = 1 \times 10^{-14} \text{ m}^2$; $\alpha = 0.05$ [1] and $R_T = 2.5 \text{ cm}$ (so we consider a square tumour), gives

$$\epsilon = 1 \times 10^{-4}, \quad \mathcal{K} = 16, \quad \mathcal{A} = 1.25, \quad \mathcal{R}_T = 1. \quad (3.18)$$

We also expect flow in the capillary to be close to Poiseuille flow, for which

$$G = \frac{3\mu\bar{u}}{R^2}, \quad (3.19)$$

thus $\mathcal{G} \approx 3$. Therefore \mathcal{K} , \mathcal{A} , \mathcal{R}_T and \mathcal{G} are $\mathcal{O}(1)$ quantities.

3.2.3 Solution of model 1

Considering first the flow in the capillary, (3.9b) gives $p = p(x)$. Then (3.9a) and (3.9c) yield, on application of (3.13),

$$u = \frac{1}{2} \frac{dp}{dx} Y^2 + b, \quad (3.20a)$$

$$v = -\frac{1}{6} \frac{d^2p}{dx^2} Y^3 - \frac{db}{dx} Y, \quad (3.20b)$$

where $b = b(x)$ is an as yet undetermined function of integration.

We now consider the tumour. Using (3.14b) and (3.16) gives

$$\frac{\partial p_T(0, 0)}{\partial x} = -\mathcal{G}. \quad (3.21)$$

Substituting (3.20a) into (3.14b,c) we obtain an expression for b ,

$$b(x) = -\left(\frac{1}{2} + \frac{1}{\mathcal{A}}\right) \frac{\partial p_T(x, 0)}{\partial x}. \quad (3.22)$$

Note that from (3.16), (3.20a), (3.21) and (3.22), the upstream flux into the capillary, Q , is given by

$$Q = \int_0^1 u \, dY \Big|_{x=0} = -\left(\frac{1}{3} + \frac{1}{\mathcal{A}}\right) \mathcal{G}. \quad (3.23)$$

Substituting (3.11b), (3.20b) and (3.22) into (3.14a) we obtain

$$\left(\frac{1}{3} + \frac{1}{\mathcal{A}}\right) \frac{\partial^2 p_T(x, 0)}{\partial x^2} = -\mathcal{K} \frac{\partial p_T(x, 0)}{\partial y}. \quad (3.24)$$

Hence we may solve Laplace's equation (3.12) on the tumour domain $0 \leq x \leq 1$, $0 \leq y \leq \mathcal{R}_T$, subject to the boundary conditions (3.14), (3.15), (3.21) and (3.24), where we are assuming that the pressure boundary layer lies at $x = 0$ to leading order. As already noted, we do not impose a boundary condition on p_T at $x = 0$, but let the value of $p_T(0, y)$, $0 \leq y \leq \mathcal{R}_T$ be a natural outcome of the solution where we impose just (3.21). Once we have determined p_T , the fluid velocity in the tumour can be calculated from (3.11); $p(x)$

and $b(x)$ can then be calculated using (3.14b) and (3.22), so we can determine the flow in the capillary from (3.20).

We implement this procedure by seeking a separable solution of (3.12). Applying (3.14) and (3.15) yields

$$p_T = A \sinh(c(x-1)) \sin(c(y - \mathcal{R}_T)), \quad (3.25)$$

where the constants A and c are fixed by conditions (3.21) and (3.24), giving

$$p_T = \frac{\mathcal{G} \sinh(c(x-1))}{c \cosh(c) \sin(c\mathcal{R}_T)} \sin(c(y - \mathcal{R}_T)), \quad (3.26)$$

where c satisfies the transcendental equation

$$\left(\frac{1}{3} + \frac{1}{\mathcal{A}}\right) c \tan(c\mathcal{R}_T) = \mathcal{K}. \quad (3.27)$$

From (3.14b) the pressure in the capillary is then

$$p(x) = -\frac{\mathcal{G} \sinh(c(x-1))}{c \cosh(c)}, \quad (3.28)$$

from (3.20) and (3.22) the flow in the capillary is

$$u(x, Y) = \frac{\mathcal{G} \cosh(c(x-1))}{\cosh(c)} \left(\frac{1}{2} - \frac{1}{2}Y^2 + \frac{1}{\mathcal{A}}\right), \quad (3.29a)$$

$$v(x, Y) = \frac{\mathcal{G} c \sinh(c(x-1))}{\cosh(c)} \left[\frac{1}{6}Y^3 - \left(\frac{1}{2} + \frac{1}{\mathcal{A}}\right)Y\right]; \quad (3.29b)$$

and the flow in the tumour is given by (3.11) as

$$u_T(x, y) = -\frac{\mathcal{K}\mathcal{G} \sinh(c(x-1))}{\cosh(c) \sin(c\mathcal{R}_T)} \sin(c(y - \mathcal{R}_T)) \quad (3.30a)$$

$$v_T(x, y) = -\frac{\mathcal{K}\mathcal{G} \sinh(c(x-1))}{\cosh(c) \sin(c\mathcal{R}_T)} \cos(c(y - \mathcal{R}_T)). \quad (3.30b)$$

Thus, the ratio of the total fluid flowing from the capillary into the tumour to the flux entering the capillary is

$$Q_a = \frac{\int_0^1 v(x, 1) dx}{\int_0^1 u(0, Y) dY} = \frac{\cosh(c) - 1}{\cosh(c)}. \quad (3.31)$$

Both the flux entering the capillary and the flux from the capillary into the tumour are proportional to the pressure gradient in the capillary, \mathcal{G} , therefore we expect the ratio, Q_a , to be independent of this parameter, \mathcal{G} , as seen in (3.31).

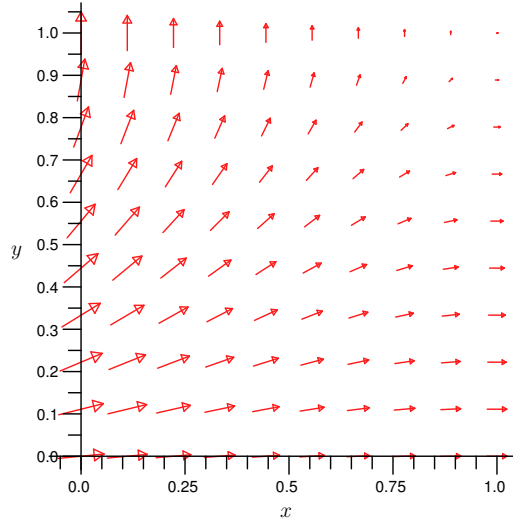


FIGURE 3: The flow in the tumour.

3.2.4 Results and limitations of model 1

Figure 3 illustrates the flow field in the tumour, and figure 4 shows the components of the fluid velocity in the capillary at different axial positions, along the capillary. We note that this velocity profile is similar to Poiseuille flow, although due to the slip condition at the interface between the capillary and tumour, the velocity is nonzero at the edges $Y = \pm 1$. The decay of the blood pressure as we move down the capillary is highlighted in figure 5.

The typical parameter values given in (3.18) yield $Q_a = 0.56$ (2 s.f.). This model thus predicts that approximately half of the fluid flowing through the capillary will enter the tumour, suggesting a viable mechanism for the virus particles to enter the tumour. (Note however that no account has been taken of the finite virus particle size, the implicit assumption being that particles will leave the capillary with the blood plasma. We address this issue in §4.)

The main shortcoming of this model is the boundary condition assumed on $x = 0$. By assuming the existence of a boundary layer in the (nondimensional) region $0 \leq x \leq x^*/L \ll 1$ we were able to avoid the discontinuous boundary condition produced by the dimensionless conditions $p_T(0, y) = 0$, $0 \leq y \leq \mathcal{R}_T$ and $\partial p_T(0, 0)/\partial x = -\mathcal{G}$. This allowed us to solve for the value of p_T on $x = x^* = 0$ (to leading order), rather than prescribing it. To solve the problem fully would require detailed consideration of this boundary layer; however for the purpose of obtaining a leading-order measure of the ratio of fluid entering the tumour relative to the total fluid flux into the capillary, this is not necessary.

This model, which does not impose the boundary conditions at $x = 0$, $0 \leq y \leq \mathcal{R}_T$, assumes that there is a boundary layer and so the pressure field is continuous. We now consider an alternative approach and impose a boundary condition which results in a discontinuity in the pressure. This second approach is probably more biologically accurate.

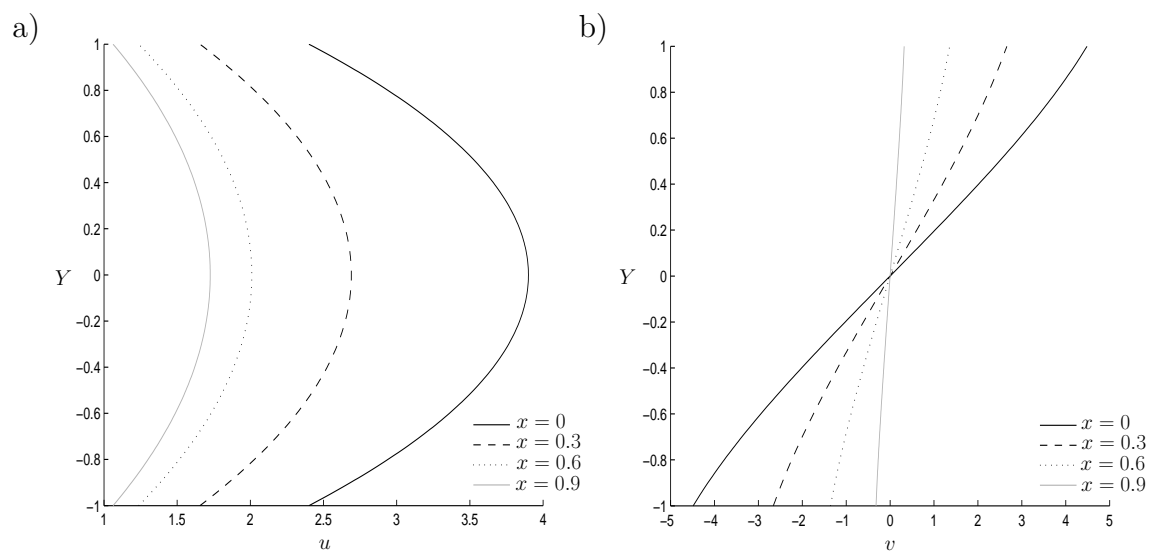


FIGURE 4: Graph illustrating the velocity profile in the capillary at various positions x down the capillary. a) Velocity in the axial direction; b) Velocity in the radial direction.

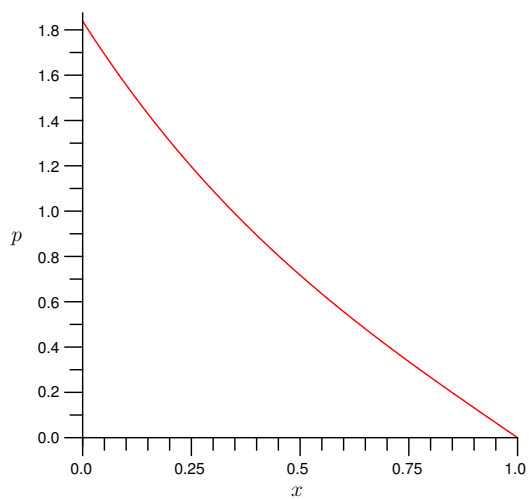


FIGURE 5: Graph illustrating the pressure profile in the capillary.

3.3 Model 2

We consider a set-up similar to model 1 above, again nondimensionalising as in (3.8), but we now apply the more physically realistic boundary condition $p_T = 0$ on $x = 0$, $0 \leq y \leq \mathcal{R}_T$. We also now prescribe the pressure gradient in the capillary in the form of a total pressure drop along its length,

$$p(0, Y) = \mathcal{P}, \quad p(1, Y) = 0, \quad (3.32a,b)$$

where $\mathcal{P} = R^2 P / \mu \bar{u} L$ is the dimensionless pressure drop, given in terms of the actual pressure drop P .

The analysis is similar to the previous model, with results (3.20) holding, however we must now solve Laplace's equation for the pressure in the tumour, (3.12) on $0 \leq x \leq 1$, $0 \leq y \leq \mathcal{R}_T$, subject to the boundary conditions

$$p_T(0, y) = 0, \quad p_T(1, y) = 0, \quad p_T(x, \mathcal{R}_T) = 0, \quad p_T(x, 0) = p(x), \quad \frac{\partial p_T(x, 0)}{\partial y} = -\mathcal{B}p''(x), \quad (3.33a-e)$$

where (3.33e) comes from (3.24) with $\mathcal{B} = (1/3 + 1/\mathcal{A})/\mathcal{K}$. Using (3.16a-c) we seek a separable solution to (3.12) to find

$$p_T(x, y) = \sum_{n=1}^{\infty} a_n \sin(n\pi x) \sinh(n\pi(y - \mathcal{R}_T)), \quad (3.34)$$

where

$$a_n = -\frac{1}{2 \sinh(n\pi \mathcal{R}_T)} \int_0^1 p(x) \sin(n\pi x) dx, \quad (3.35)$$

from (3.16d). Substituting into (3.16e) then gives the following integro-differential equation for the capillary pressure $p(x)$,

$$\frac{n\pi \sin(n\pi x) \cosh(n\pi \mathcal{R}_T)}{2 \sinh(n\pi \mathcal{R}_T)} \int_0^1 p(x) \sin(n\pi x) dx = \mathcal{B}p''(x). \quad (3.36)$$

Writing $p(x)$ in the form

$$p(x) = \mathcal{P}(1 - x) + g(x), \quad (3.37)$$

with $g(0) = g(1) = 0$, we may seek a Fourier series solution for $g(x)$

$$g(x) = \sum_{n=0}^{\infty} b_n \sin(n\pi x). \quad (3.38)$$

Substituting (3.37) and (3.38) into (3.36) gives

$$b_n = -\frac{2\mathcal{P} \coth(n\pi \mathcal{R}_T)}{n\pi \coth(n\pi \mathcal{R}_T) + n^2 \pi^2 \mathcal{B}}, \quad (3.39)$$

and substituting (3.37) into (3.35) gives

$$a_n = -\frac{2\mathcal{P}}{n\pi \sinh(n\pi \mathcal{R}_T)} - \frac{\mathcal{P}}{\sinh(n\pi \mathcal{R}_T)} b_n \quad (3.40)$$

$$= \frac{2\mathcal{P}}{n\pi \sinh(n\pi \mathcal{R}_T)} \left(-1 + \frac{\mathcal{P} \coth(n\pi \mathcal{R}_T)}{\coth(n\pi \mathcal{R}_T) + n\pi \mathcal{B}} \right). \quad (3.41)$$

Hence the pressure in the tumour, p_T , is given by (3.34), where the series coefficients a_n are given by (3.41).

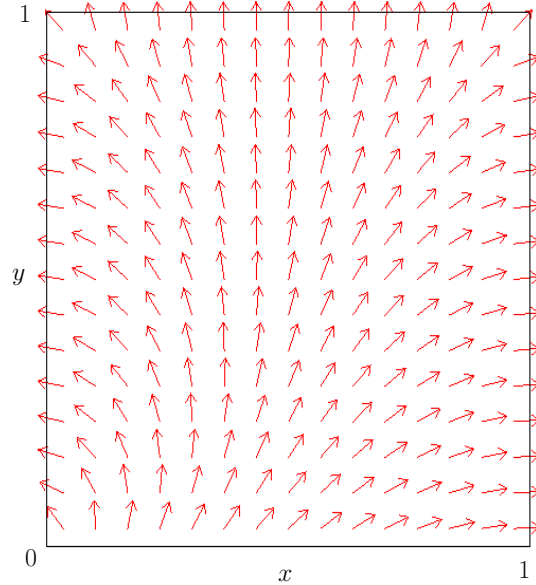


FIGURE 6: The direction of the flow in the tumour. (Note, in this figure the arrow lengths are not related to the flow speed.)

3.3.1 Results and limitations of model 2

Figure 6 illustrates the direction of the flow within the tumour. Comparing figures 6 and 3, we see the main difference between the two models is the flow pattern near $x = 0$ for $0 \leq y \leq \mathcal{R}_T$. In model 2, to achieve the boundary condition $p_T(0, y) = 0$, we observe a change in direction of the flow, which is perhaps more physically realistic. However, the solution obtained for p_T is less mathematically tractable, because p_T is discontinuous at $(0, 0)$ due to the discontinuity between the boundary condition $p_T(0, y) = 0$, for $0 \leq y \leq \mathcal{R}_T$, and the condition $p_T(0, 0) = \mathcal{P}$. This results in numerical difficulty in extracting the fluid velocities, and hence in obtaining a measure of the flux of fluid into the tumour.

4 Flow into a gap between endothelial cells

In this section we investigate the local problem of flow into a single gap between the endothelial cells. There is a range of possible gap sizes, therefore we consider separately the cases in which the small rigid virus particles do and do not affect the local flow into the gap.

4.1 Gaps much larger than the virus particle

Here we assume that the virus particles may be treated as point particles, which are simply advected with the flow, having no influence upon it. We consider the flow in the neighbourhood of an isolated gap in the endothelium. We model the gap as a deep circularly-cylindrical hole in the endothelial wall, assuming that the gap radius is sufficiently small relative to the radius of curvature of the capillary that the local geometry of

the capillary wall plus gap may be approximated by a circular well in a flat plane, with shear flow above parallel to the plane and over the gap.

This local fluid dynamical problem was studied by Tutty [10], who solved for shear Stokes flow in a half-space over a circularly cylindrical hole perpendicular to the bounding plane. In addition to the imposed shear, flow was driven by suction into the hole, with Poiseuille flow developing far down the hole. (The application considered by Tutty was flow through an artery with a small side branch, the primary concern being the shear forces applied to the walls of blood vessels in mammals.) The linearity of Stokes flow means that the problem can be split into two independent two-dimensional subproblems: the axisymmetric problem with fluid being purely sucked down the hole, with specified flux; and a second problem where the shear flow in the half-space passes a hole with no suction present.

Tutty [10] showed that the imposed pure shear flow produces a series of eddies running down the hole, whose strength decays exponentially with distance down the hole. With both shear and suction combined, the family of solutions is characterised by the parameter Q_b , the relative strength of suction down the hole versus shear flow over it.

Figure 7 (from [10]) shows a typical streamline pattern. Flux into the hole (driven by the lower pressure within the tumour, in our application) suppresses the eddies that are present when the flow is purely shear-driven. In fact with $Q_b > 0.027$ all eddies are suppressed, and even only a small flux into the gap suppresses all but the first eddy. When left intact, this first eddy is reduced and compressed against the upstream wall of the hole (figure 7a). Below a dividing stream surface cross-section all the fluid is sucked into the hole. Figure 8 shows this dividing stream surface cross-section for several values of the suction parameter Q_b . Following it back upstream in the shear, the dividing surface becomes parallel to the plane. The size of the entrainment region beneath the dividing stream surface increases with increasing suction. Figure 9 shows a three-dimensional representation of the dividing stream surface. In our application, with the assumption of virus particles purely advected with the flow, particles that start out within the entrainment region will enter the gap, and thus the tumour. For a given shear-rate within the capillary, and given pressure drop from the capillary to the tumour, the size of the parameter Q_b can be estimated, and, together with knowledge about the distribution of virus particles across the capillary, Tutty's results could be used to estimate directly the quantity of virus particles entering the tumour under given conditions.

4.2 Gap size comparable to the virus particle size

The above analysis, using Tutty's model [10], will only be valid if the virus particles used are small compared to the size of the gaps in the endothelium. If the particles are comparable to the gap size, the effect they have on the local flow near the gap will be important and the interactions of virus particles with the flow must be considered. Although adhesive forces may be present between the virus particle and the wall, we neglect these forces for simplicity. A relevant local problem was considered by Wu *et al.* [11], who considered the motion of a single rigid neutrally-buoyant sphere in a shear Stokes flow past an infinite thin wall with a circular aperture (not an infinite well as in the work of Tutty [10]). In addition to the shear, flow was also driven by an imposed suction through the hole.

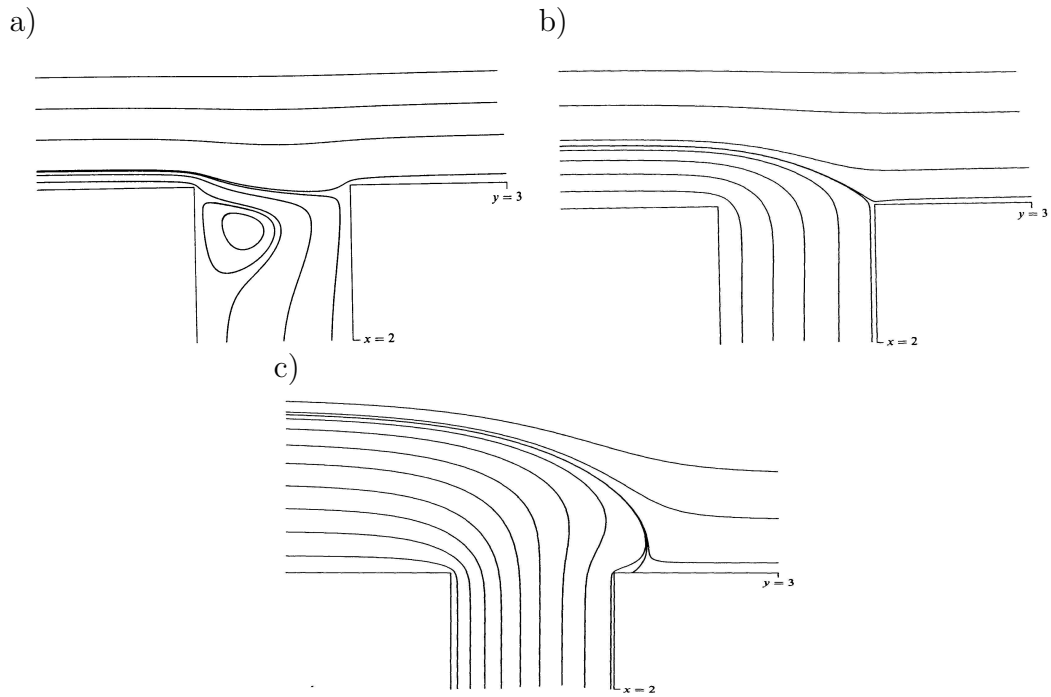


FIGURE 7: The streamlines for which there is shear flow along the capillary and flux into the gap, from [10]; a) $Q_b = 1/200$, b) $Q_b = 0.11$, c) $Q_b = 2$

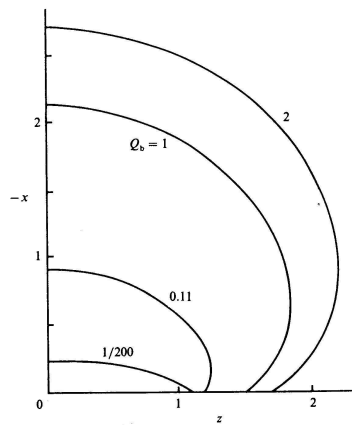


FIGURE 8: The entrainment region at $y = -3$, from [10].

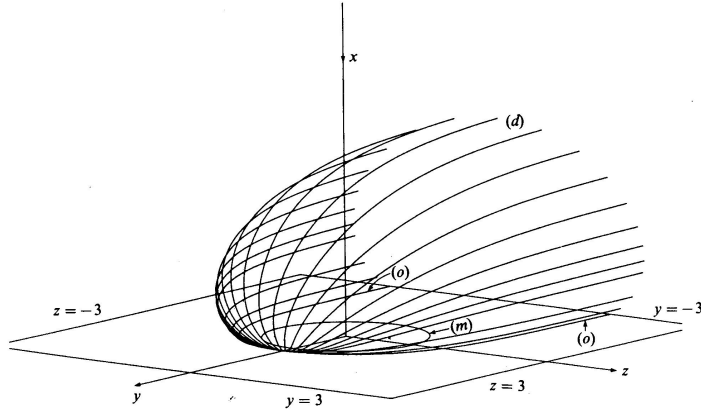


FIGURE 9: The dividing streamlines for $Q_b = 2$, from [10]; (o) denotes the main tube wall and (m) denotes the gap in the endothelial cells.

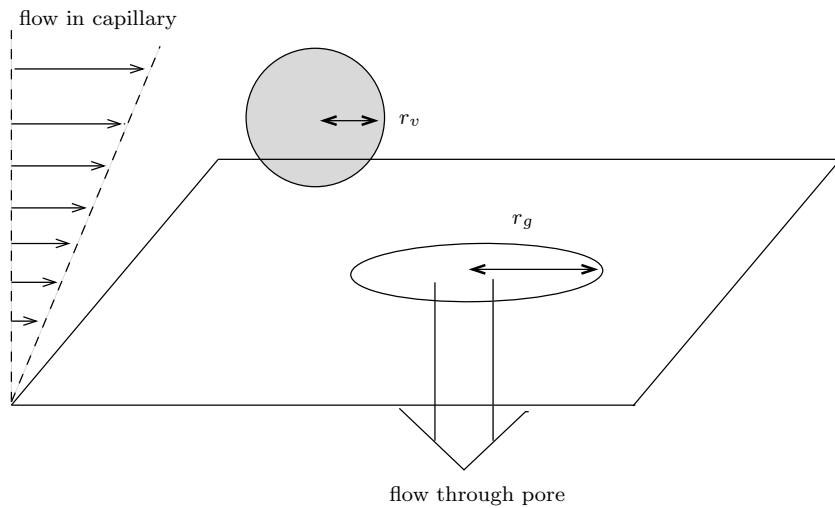


FIGURE 10: The particle and the hole.

Almost as above, we may approximate the local geometry of capillary plus a single isolated gap by a half-space with a circular aperture, with shear flow above and an imposed suction through the aperture to model the pressure difference between tumour and capillary. Treating the virus particle as a uniform, neutrally buoyant, rigid sphere, we have the situation sketched in figure 4.2, and the work of Wu *et al.* [11] outlined above is applicable.

Appealing to the linearity of the Stokes equations, Wu *et al.* [11] superimposed a Sampson flow (suction through a circular aperture in an infinite thin wall) onto a shear flow (an approximation to the base flow neglecting the particle), and combined with the flow caused by the particle to give the total flow field. They then solved this problem numerically to find the force and torque exerted by the fluid on the sphere, which allowed them to calculate sphere trajectories, and hence the conditions for particle capture for the flow. They identified two key parameters: a geometrical parameter r_v/r_g , where r_v is the radius of the virus particle and r_g is the radius of the aperture, and (cf Tutty [10])

a parameter characterising the effects of suction versus shear, defined to be

$$Q = \frac{\text{flux in pore}}{\text{flux in capillary}}. \quad (4.1)$$

By calculating the dividing streamlines (which form a dividing streamsurface) we may determine the particle capture tube, which encloses the volume of particle trajectories that enter the hole. Wu *et al.* [11] find that there are a finite range of upstream particle trajectories that bring the particles close to the wall before they “roll” into the hole. In this report we assume the particle trajectory is aligned with the centre of the hole for simplicity (probably a reasonable assumption since there are many gaps in the wall, and a particle is much more likely to fall into a gap with which it is perfectly aligned).

The location of the dividing streamlines varies with Q , and r_v/r_g . If the suction is strong the particle could come close to the wall downstream of the hole and roll backwards into the hole, as shown in figure 11. For intermediate suction strength the dividing streamline no longer impinges on the wall but enters the hole as shown in Figure 12. As Q decreases towards $Q_{\min}(r_v/r_g)$, this dividing streamline moves upstream until it impinges on the upstream rim of the hole for $Q = Q_{\min}(r_v/r_g)$. Therefore, for $Q < Q_{\min}(r_v/r_g)$ no particles enter the hole. Wu *et al.* [11] calculate $Q_{\min} = 0.04$ for $r_v/r_g = 1/2$.

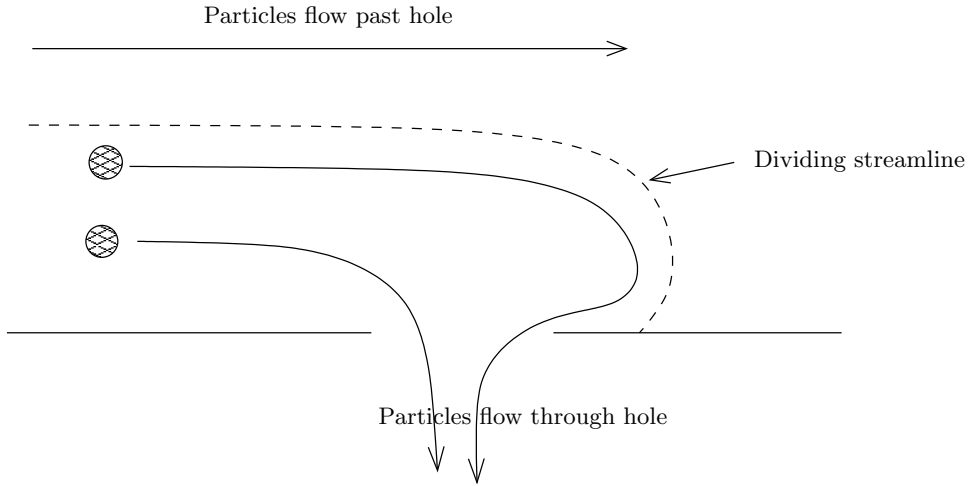


FIGURE 11: A cross-section of the particle capture tube for large Q , the particle can flow past the hole before being captured and pulled back.

4.2.1 Application to virus particle capture by tumour

Considering Sampson flow through the gap in the endothelial wall gives [6]

$$Q = \frac{\Delta p r_g^3 / 3\mu}{\pi R^2 \bar{u}}, \quad (4.2)$$

from (4.1), where Δp is the pressure drop from the capillary to the tumour, r_g is the gap radius, μ is the blood (plasma) viscosity, R is the capillary radius and \bar{u} is the mean axial velocity in the capillary. Choosing typical values $\Delta p = 10$ mm Hg, $r_g = 2r_v$ (a worst case

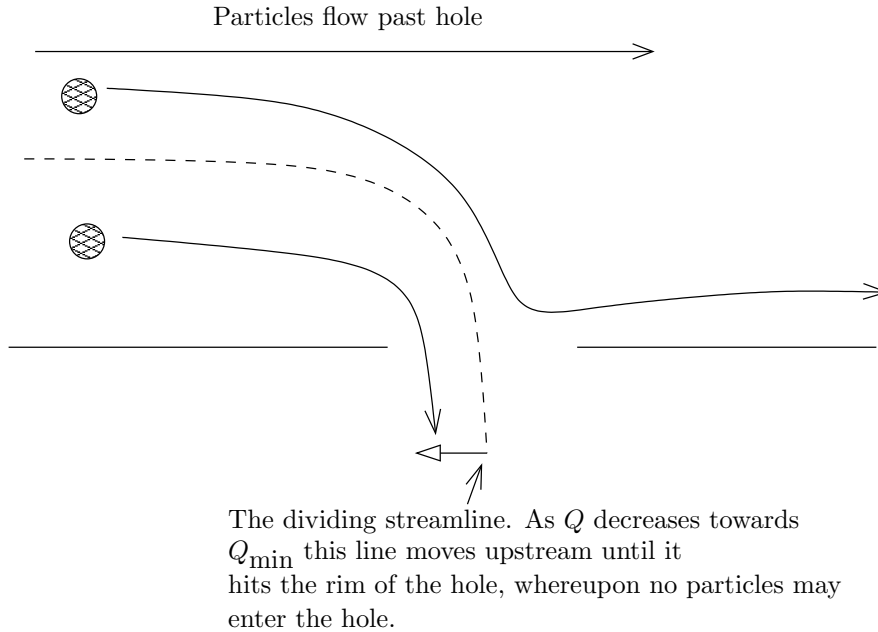


FIGURE 12: A cross-section of the particle capture tube for an intermediate value of Q .

scenario in the sense of virus-capture difficulty), $r_v = 100 \text{ nm}$, $\mu = 1.35 \times 10^{-3} \text{ kgm}^{-1} \text{ s}^{-1}$ and $\bar{u} = 0.1 \text{ mms}^{-1}$, gives

$$Q = 0.13 \quad (2 \text{ s.f.}) \quad > Q_{\min} \quad (4.3)$$

and so some particle capture will occur. This calculation is based on a larger virus-to-gap ratio than would typically be the case. Since we expect Q_{\min} to increase with r_v/r_g (thus decreasing with r_g), and since Q increases with r_g (see (4.2)) this is in some sense the ‘worst case scenario’. We thus anticipate a non-empty particle capture tube, and so if the virus comes sufficiently close to the gap in the endothelial wall the particle will enter the tumour, even in this worst case. To evaluate the ‘cost’ of using the larger (but more effective) viruses under consideration we would need to know how Q_{\min} varies with r_v/r_g . Unfortunately, Wu *et al.* [11] do not provide data on the variation of Q_{\min} with r_v/r_g ; this could be calculated by following their computational methods, however this is beyond the scope of the present report.

5 Encapsulated viruses

Thus far the work in this report has assumed either that the virus particles are advected passively with the flow (an assumption valid in relatively large vessels where diffusion of the particles is negligible), or that they behave as rigid spheres when they interact with the flow in the vessel. However, as mentioned in the Introduction, an important class of virus particles are *encapsulated* within a loose membrane coating. Essentially such viruses behave as small rigid particles, contained within a fluid-filled inextensible membrane bag (see figure 13, which also gives typical dimensions).

When in the regime where they are not passively advected with the flow, such viruses will behave very differently from rigid particles in the way they interact with the flow.

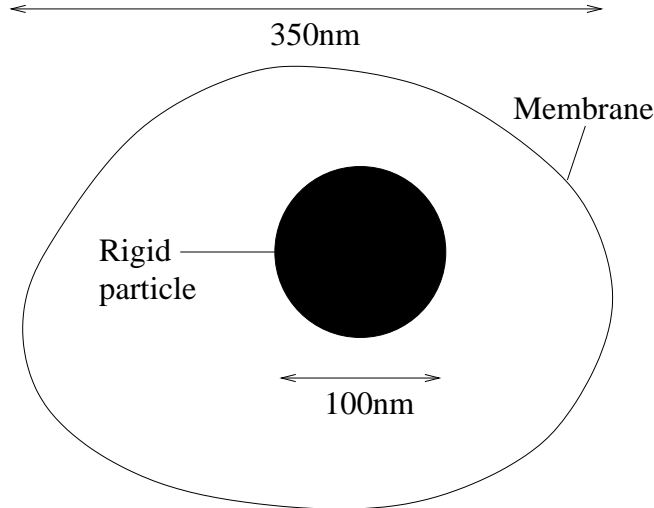


FIGURE 13: Sketch of an encapsulated virus, with typical dimensions.

In particular, we expect them to behave very differently in the vicinity of a vessel wall, which is, of course, crucial for their capture by the tumour. In this section we consider how such particles might be modelled, and suggest some possible approaches towards solving the resulting models.

5.1 Encapsulated virus near a wall: Lubrication problem

When an encapsulated virus such as that shown in figure 13 is sufficiently near a vessel wall, there is a thin layer of liquid between the virus and the wall. The set-up is sketched in figure 14, which shows the whole geometry, and figure 15, which shows the local “lubrication” geometry. For simplicity a two-dimensional problem is considered. The vessel wall lies along $y = 0$, and the solid virus particle is centred at position $(X_3(t), Y_3(t))$, which must be determined as part of the solution, as well as the unknown position of the outer virus membrane.

Between the vessel wall at $y = 0$ and the lower membrane surface at $y = H_1(x, t)$ (labelled region 1 in figure 15) is a layer of blood, of viscosity μ_1 . Inside the virus, between the membrane at $y = H_1(x, t)$ and the rigid virus particle surface at $y = H_2(x, t)$ (labelled region 2 in figure 15) is a layer of virus cytoplasm, of viscosity μ_2 .

If R denotes a typical membrane radius, U denotes a typical oncoming (axial) flow speed, and $\epsilon = h_o/R$; the following scalings are employed:

$$x = \sqrt{\epsilon}R\tilde{x}, \quad y = \epsilon R\tilde{y}, \quad u = U\tilde{u}, \quad v = \sqrt{\epsilon}U\tilde{v}, \quad p_i = \frac{\mu_i U}{\epsilon^{3/2}R}\tilde{p}_i. \quad (5.1)$$

Defining a capillary number $\text{Ca} = \mu_1 U / (\epsilon^{3/2} \gamma)$, the leading-order equations and boundary conditions for the flow and membrane shape in the dimensionless variables become (after dropping the tildes)

$$\left. \begin{aligned} p_{ix} &= u_{iyy} \\ p_{iy} &= 0 \\ u_{ix} + v_{iy} &= 0 \end{aligned} \right\} \quad i = 1, 2, \quad (5.2)$$

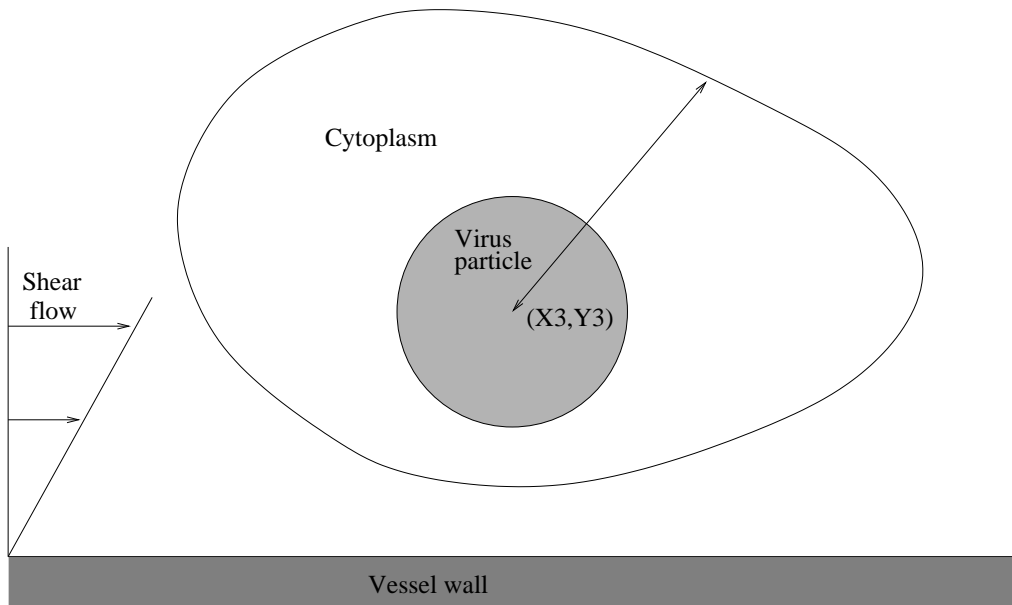


FIGURE 14: Encapsulated virus near wall in shear flow.

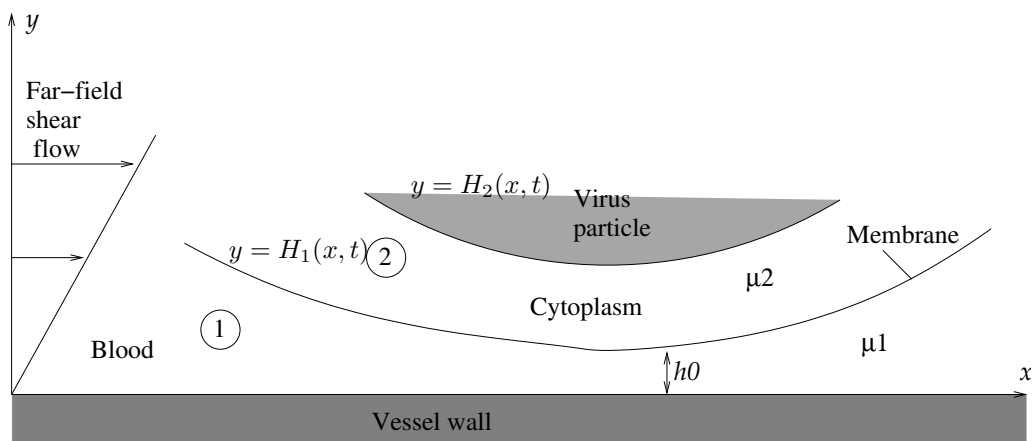


FIGURE 15: Sketch of “lubrication” geometry.

representing the lubrication equations holding in each region;

$$\left. \begin{aligned} H_{1t} + u_{1,2}H_{1x} &= v_{1,2} \\ -p_1 + \bar{\mu}p_2 &= \frac{1}{Ca}H_{1xx} \\ u_{1y} - \bar{\mu}u_{2y} &= T_s \\ \mathbf{u}_1 = \mathbf{u}_2 &= \mathbf{U}_m \end{aligned} \right\} \text{ on } y = H_1(x, t), \quad (5.3)$$

representing a kinematic condition at the deformable membrane, normal and tangential stress balances respectively (where $\bar{\mu} = \mu_2/\mu_1$ is the viscosity contrast of the two fluids, T is the membrane tension, s is arc length and \mathbf{U}_m is the velocity of the membrane) and the no-slip condition;

$$\mathbf{u}_2 = \mathbf{v}_p = \dot{\mathbf{X}}_3 + \boldsymbol{\omega} \wedge (\mathbf{x} - \mathbf{X}_3) \quad \text{at } y = H_2(x, t), \quad (5.4)$$

representing continuity of velocity at the surface of the rigid virus core (\mathbf{v}_p represents its translational velocity and $\boldsymbol{\omega}$ its angular velocity), and

$$\mathbf{u}_1 = \mathbf{0} \quad \text{at } y = 0. \quad (5.5)$$

Far-field conditions in regions 1 and 2 and a torque balance on the rigid virus core, along with matching with the outer problem, complete the problem specification. This problem will be studied further in due course, but its solution is beyond the scope of this preliminary report.

5.2 The “full” problem: Formulation

Another idealised problem that can be considered, which has the advantage of enabling the whole membrane to be modelled, is to solve for a fluid-filled bag within the blood flow. In this case we neglect the solid virus core, and again consider a two-dimensional model for simplicity.

Since Reynolds numbers for blood flow in a capillary are typically small, and certainly the Reynolds number for the cytoplasm within the bag will be small, both fluids may be modelled using the Stokes (slow-flow) equations.

The neatest formulation for this problem is in terms of the Airy stress function A for both fluid regions, in terms of which the stress tensor in the fluid may be written as

$$\boldsymbol{\sigma} = \begin{pmatrix} A_{yy} & -A_{xy} \\ -A_{xy} & A_{xx} \end{pmatrix}. \quad (5.6)$$

Using subscripts 1 and 2 to denote the blood and cytoplasm regions respectively, \mathbf{n} to denote the vector in the direction of the outward normal to the membrane (with n the corresponding scalar coordinate), $\mathbf{t}(s)$ to denote the anticlockwise tangent vector at the membrane surface (with s the corresponding scalar coordinate), and $\gamma(s)$ to denote the tension in the membrane, the problems to be solved in each region are as follows [7]:

$$\nabla^4 A_i = 0 \quad \text{in region } i, \quad i = 1, 2, \quad (5.7a)$$

$$[A]_2^1 = 0, \quad (5.7b)$$

$$\left[\frac{\partial A}{\partial n} \right]_2^1 = \gamma(s), \quad (5.7c)$$

$$\frac{\partial}{\partial s} (\mathbf{u}_m \cdot \mathbf{t}) = 0, \quad (5.7d)$$

the last condition representing the inextensibility of the membrane, with \mathbf{u}_m the membrane velocity, which must also equal the fluid velocity at the boundary on either side of the membrane.

The problem is closed by specifying far-field conditions on the velocity in region 1, and an initial condition on the geometry. In general one has to solve for A_1 , A_2 , $\gamma(s)$ and the membrane position.

5.3 Concluding remarks

The membrane encapsulating the virus greatly complicates the fluid dynamics of the full virus transport problem, making it much harder to analyse mathematically. The problems outlined in sections 5.1 and 5.2 above represent realistic steps towards a more tractable problem, but are still far from trivial to solve. Furthermore, one might argue that, in simplifying to obtain a more tractable model, we are losing sight of the situation of most interest, when the virus is near a gap in the wall, experiencing a slight suction towards it due to the lower pressure within the tumour. Such a suction force could be incorporated into the lubrication model above without difficulty, but the issue of how a virus might manoeuvre itself through a gap (which might entail it deforming to squeeze through) is clearly very difficult to address. Nonetheless, problems of the kind outlined above should (when solved) provide valuable insight into the difference in behaviour between encapsulated and non-encapsulated viruses.

6 Conclusions

In this report we focused on three different aspects of the biological problem. Firstly, in §3 we studied the macroscale problem of flow through an entire tumour. We modelled the tumour as a porous medium and we assumed the virus particles are point particles which are passively advected by the blood flow. Although there were physical limitations in the tractable boundary conditions, we found a significant proportion of the blood (and therefore the virus particles) leaks from the capillary into the tumour.

Secondly, in §4 we studied the flow into a single gap between endothelial cells. Assuming the virus particles are small compared with the size of the gap and are passively advected with the blood flow, we found virus particles within an entrainment region would enter the tumour. The size of the entrainment region, and therefore the number of virus particles entering the tumour, increases with increasing suction into the gap. However if the gap size is comparable to the virus particle size, the presence of the virus particle influences the blood flow. In this case, the suction into the gap is sufficient to capture some of the virus particles.

Finally in §5 we studied the encapsulated virus particle. Stresses from the blood flow will deform the virus's membrane. Thus the physical properties of the virus particle influence its motion close to the wall and this motion may significantly affect the number of virus particles which enter the tumour.

7 Participants

The following people were involved with this problem during the study group: L R Band, R J S Booth, C J W Breward, L J Cummings, R J Dyson, K Fisher, I M Griffiths, P D Howell, M D Johnson, J R King, D Miroshnychenko, J P Moles, J R Ockendon, G W Richardson, C M Stott, Z S J Tayler and S L Waters.

References

- [1] Beavers, G.S. & Joseph, D.J. 1967 Boundary conditions at a naturally permeable wall. *J. Fluid. Mech.* **30**, 197–207.
- [2] Feng, D., et al. 1999 Pathways of macromolecular extravasation across microvascular endothelium in response to VPF/VEGF and other vasoactive mediators. *Microcirculation.* **6(1)** 23–44.
- [3] Fisher, K.D., et al. 2001 Polymer-coated adenovirus permits efficient retargeting and evades neutralising antibodies. *Gene Ther.* **8(5)** 341–8.
- [4] Fowler, A.C. 1997 *Mathematical Models in the Applied Sciences*. Cambridge University Press.
- [5] Green, N.K., et al., Extended plasma circulation time and decreased toxicity of polymer-coated adenovirus. *Gene Ther.* **11(16)** 1256–63.
- [6] Happel, J. & Brenner, H. 1973 *Low Reynolds Number Hydrodynamics*, 2nd edn. Noordhoff.
- [7] KING, J.R. D. Phil. Thesis, *University of Oxford*, (1986).
- [8] Seymour, L.W. 1992 Passive tumor targeting of soluble macromolecules and drug conjugates. *Crit. Rev. Ther. Drug Carrier Syst.* **9(2)** 135–87.
- [9] Thorne, S.H. & Kirn D.H. 2004 Future directions for the field of oncolytic virotherapy: a perspective on the use of vaccinia virus. *Expert Opin Biol Ther.* **4(8)** 1307–1321.
- [10] Tutty, O.R. 1988 Flow in a tube with a small side branch. *J. Fluid Mech.* **191**, 79–109.
- [11] Wu, W-Y, Weinbaum, S. & Acrivos, A. 1992 Shear flow over a wall with suction and its application to particle screening. *J. Fluid Mech.* **243**, 489–518.